Cellular/Molecular

Isolation of Somatic Na^+ Currents by Selective Inactivation of Axonal Channels with a Voltage Prepulse

Lorin S. Milescu,[1,2] Bruce P. Bean,[1] and Jeffrey C. Smith[2]

[1]Department of Neurobiology, Harvard Medical School, Boston, Massachusetts 02115, and [2]Cellular and Systems Neurobiology Section, National Institute of Neurological Disorders and Stroke, National Institutes of Health, Bethesda, Maryland 20892

We present a simple and effective method for isolating the somatic Na^+ current recorded under voltage clamp from neurons in brain slices. The principle is to convert the axon from an active compartment capable of generating uncontrolled axonal spikes into a passive structure by selectively inactivating axonal Na^+ channels. Typically, whole-cell currents from intact neurons under somatic voltage clamp contain a mixture of Na^+ current and axial current caused by escaped axonal spikes. We found that a brief prepulse to voltages near spike threshold evokes the axonal spike, which inactivates axonal but not somatic channels. A subsequent voltage step then evokes only somatic Na^+ current from electrotonically proximal sodium channels under good voltage-clamp control. Simulations using a neuron compartmental model support the idea that the prepulse effectively inactivates currents from the axon and isolates well controlled somatic currents. Na^+ currents recorded from cortical pyramidal neurons in slices, using the prepulse, were found to have voltage dependence nearly identical to that of currents recorded from acutely dissociated pyramidal neurons. In addition, studies in dissociated neurons show that the prepulse has no visible effect on the voltage dependence and kinetics of Na^+ currents elicited by the subsequent voltage step, only decreasing the amplitude of the currents by 10–20%. The technique was effective in several neuronal types in brain slices from male and female neonatal rats and mice, including raphé neurons, cortical pyramidal neurons, inferior olivary neurons, and hypoglossal motoneurons.

Introduction

Voltage-gated sodium (Na_v) channels underlie the spiking activity of mammalian central neurons. The neuronal function of Na_v channels is typically inferred from their kinetic properties measured in voltage clamp (Hodgkin and Huxley, 1952). In principle, whole-cell recording (Hamill et al., 1981) from the acute brain slice preparation (Edwards et al., 1989) is an ideal method for defining channel properties in central neurons with physiological and structural integrity. Unfortunately, lack of space clamp makes it very difficult to obtain well controlled Na^+ currents from intact neurons *in situ*. Neurons are multicompartmented structures, and voltage clamping the soma is not sufficient for controlling the membrane potential in other compartments (Rall and Segev, 1985; Spruston et al., 1993; White et al., 1995; Hartline and Castelfranco, 2003; Bar-Yehuda and Korngreen, 2008). This is a particular difficulty for Na_v channels, because these are present at high density in the axon initial segment (Osorio et al., 2005; Castelli et al., 2007; Kole et al., 2008; Royeck et al., 2008; Diwakar et al., 2009), which constitutes an electrotonically distinct compartment whose voltage can deviate dramatically from that in the soma (Stuart et al., 1997; Kole et al., 2008). As a result, electrotonically remote Na_v channels, relative to the point of current injection, escape voltage clamp and generate unclamped currents. Because of this, Na^+ currents could be recorded with good voltage control from central neurons *in situ* in only a few unusually favorable cases (Magistretti et al., 2006; Enomoto et al., 2007).

The space-clamp problem can be circumvented by recording from reduced neuronal preparations, such as acutely dissociated neurons or nucleated patches. However, recording well controlled Na^+ currents directly from healthy neurons in brain slice preparations could be of great advantage. For example, neuronal identity can be easily established in the slice, and Na_v channel kinetic properties can be correlated with neuronal morphology and network location. *In situ* recording could also facilitate the study of transmitter modulation of sodium currents by helping preserve biochemical pathways.

We provide here a simple yet effective solution to the space-clamp problem. The principle is to convert the axon from an active compartment capable of generating uncontrolled axonal spikes into a passive structure by selectively inactivating axonal Na_v channels with a voltage prepulse. The idea came from the observation that, in depolarizing steps to subthreshold potentials, an out-of-control current spike occurs within the first 5–10 ms, but for the following 20–50 ms the current appears well controlled. This spike represents the axial current caused by the voltage difference between soma and axon, which transiently occurs when the electrotonically remote and out-of-control axonal Na_v channels generate an axonal spike. These channels would briefly experience strongly inactivating potentials during the

Received Dec. 10, 2009; revised March 23, 2010; accepted April 18, 2010.

This work was supported by the Intramural Research Program of the National Institutes of Health (NIH), National Institute of Neurological Disorders and Stroke and by NIH R01 Grant NS36855 to B.P.B. We thank our colleagues for suggestions, particularly Drs. Mirela Milescu (NIH, Bethesda, MD), Reese Scroggs (University of Tennessee, Memphis, TN), and Joel Tabak (Florida State University, Tallahassee, FL). Dr. Ruli Zhang (NIH, Bethesda, MD) assisted with animal procedures.

Correspondence should be addressed to Lorin S. Milescu, Department of Neurobiology, Harvard Medical School, 220 Longwood Avenue, Goldenson Building, Room 420, Boston, MA 02115. E-mail: Lorin_Milescu@hms.harvard.edu.

DOI:10.1523/JNEUROSCI.6136-09.2010

 0270-6474/10/307740-09$15.00/0

spike. In contrast, somatic Na_v channels would experience their local potential maintained by voltage clamp to subthreshold values, where inactivation is slow. In the following, we demonstrate how the out-of-control axonal spike can be used to our advantage to inactivate axonal Na_v channels and isolate a well controlled somatic Na^+ current from the axial current.

Materials and Methods

Animal procedures. All animal procedures were approved by the National Institute of Neurological Disorders and Stroke Animal Care and Use Committee.

Slices. In vitro medullary slice preparations containing midline raphé neurons, inferior olivary neurons, and hypoglossal motoneurons were obtained from postnatal (P0–P4) Sprague Dawley rats (Koshiya and Smith, 1999). Cortical slices containing pyramidal neurons were obtained from postnatal (P7–P9) Swiss-Webster mice. Either medulla or brain was dissected in artificial CSF (aCSF) containing the following (in mM): 124 NaCl, 25 $NaHCO_3$, 3 KCl, 1.5 $CaCl_2$, 1.0 $MgSO_4$, 0.5 NaH_2PO_4, and 30 D-glucose, equilibrated with 95% O_2 and 5% CO_2 (pH 7.4 ± 0.05 at room temperature). Slices (300–400 μm thick) were transferred to a recording chamber mounted on a microscope stage, and superfused with aCSF at room temperature.

Dissociated neurons. Pyramidal cortical neurons were dissociated from postnatal (P7–P9) Swiss-Webster mice according to previously published procedures (Carter and Bean, 2009). Droplets of suspension containing dissociated neurons were transferred to the recording chamber. After waiting 1 or 2 min to allow neurons to sediment and stick to the glass bottom, the chamber was superfused with aCSF at room temperature.

Neuron identification. Brainstem neurons (raphé, olivary, and hypoglossal motoneurons) were selected based on their location in the slice. In slices, cortical pyramidal neurons were selected based on their characteristic morphology and location in cortical layer V. Dissociated pyramidal neurons were identified by their larger size, pyramidal shape, and presence of a thick apical dendrite stump at one end and thinner stumps of basal dendrites at the other end. All experiments were done under infrared-differential interference contrast (IR-DIC) visualization.

Solutions. Pipettes were filled with a solution containing the following (in mM): 100 Cs-gluconate (prepared from CsOH and gluconic acid), 10 tetraethylammonium chloride (TEA-Cl), 5 4-aminopyridine (4-AP), 10 EGTA, 1 $CaCl_2$, 10 HEPES, 4 Mg-ATP, 0.3 Na_3-GTP, 4 Na_2-phosphocreatine, 4 NaCl, pH 7.4, adjusted with CsOH (285 ± 5 mOsm/L). To reduce the size of Na^+ currents, in some experiments a 50 mM Na^+ solution was used containing 70 Cs-gluconate, 30 Na-gluconate, 10 TEA-Cl, 5 4-AP, 10 EGTA, 1 $CaCl_2$, 10 HEPES, 4 Mg-ATP, 0.3 Na_3-GTP, 10 Na_2-phosphocreatine.

Pharmacology. $CdCl_2$ (120 μM) and (in some slice experiments) 1,2,3,4-tetrahydro-6-nitro-2,3-dioxo-benzo[*f*]quinoxaline-7-sulfonamide (NBQX; 10 μM) were added to the superfusing aCSF to block Ca^{2+} currents and inhibit synaptic transmission. TTX was added to the superfusing aCSF at 50 nM to reduce the magnitude of Na^+ currents or at 1 μM to completely inhibit them. All reagents were purchased from Sigma-RBI.

Electrophysiology. Electrodes (5–7 MΩ) were pulled from borosilicate glass and coated with Sylgard to reduce capacitive transients. Series resistance (R_s) was typically 9–15 MΩ in slices and 7–12 MΩ in dissociated neurons. Cells with $R_s > 15$ MΩ were discarded. R_s was compensated 80% (2 μs response time), and the compensation was readjusted before each voltage-clamp protocol. A measured liquid junction potential of ≈8 mV was corrected on-line. Somatic whole-cell recordings were obtained with a HEKA EPC10 double patch-clamp amplifier. Data were low-pass filtered at 40 kHz and digitally sampled at 100 kHz using the amplifier's built-in digitizer, controlled by Pulse software. Voltage-clamp protocols were constructed and applied with Pulse software. Leak currents were subtracted using the P/n protocol. In some cases, the protocols were repeated under bath-applied TTX to better isolate Na^+ currents using TTX subtraction. In all protocols, the intersweep interval was 2 s at −80 mV. Patch stability was monitored in all protocols, and unstable recordings were discarded.

Data analysis and statistics. We used custom-made scripts in the QuB software (www.qub.buffalo.edu) to process the voltage-clamp data and to implement ion channel and cellular models and run simulations. Statistics and curve fitting were done with Prism 4.0 software.

Ion channel models. For the Na_v channel, we used the allosteric model proposed by Kuo and Bean (1994):

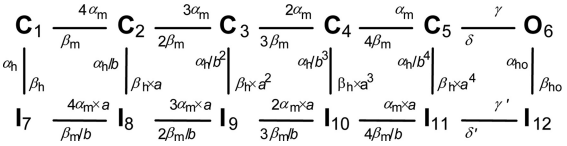

(1)

For the K_v channel, we used the Markov equivalent of the widely used n^4 Hodgkin–Huxley model:

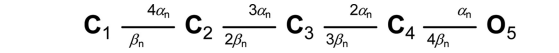

(2)

For any transition between states *i* and *j*, the rate constant has the form

$$k = k_0 \times \exp(k_1 \times V), \tag{3}$$

where k_0 is the rate constant at zero potential (ms^{-1}), k_1 is the voltage dependence (mV^{-1}), and V is the membrane potential (mV).

Neuron compartmental model. The differential equations describing the dynamics of the compartmental model (see Fig. 2) for the soma are

$$C_m \times \frac{dV_m}{dt} = -I_m - I_{mx} - I_c, \tag{4}$$

$$\frac{d\mathbf{P}_{Na,m}}{dt} = \mathbf{P}_{Na,m} \times \mathbf{Q}_{Na}, \tag{5}$$

and

$$\frac{d\mathbf{P}_{K,m}}{dt} = \mathbf{P}_{K,m} \times \mathbf{Q}_{K}, \tag{6}$$

and those for the axon are

$$C_x \times \frac{dV_x}{dt} = -I_x + I_{mx}, \tag{7}$$

$$\frac{d\mathbf{P}_{Na,x}}{dt} = \mathbf{P}_{Na,x} \times \mathbf{Q}_{Na}, \tag{8}$$

and

$$\frac{d\mathbf{P}_{K,x}}{dt} = \mathbf{P}_{K,x} \times \mathbf{Q}_{K}, \tag{9}$$

where

$$I_m = G_{Na,m} \times P_{o,Na,m} \times (V_m - V_{Na}) + G_{K,m} \times P_{o,K,m} \times (V_m - V_K) + G_{Lk,m} \times (V_m - V_{LK}), \tag{10}$$

$$I_x = G_{Na,x} \times P_{o,Na,x} \times (V_m - V_{Na}) + G_{K,x} \times P_{o,K,x} \times (V_m - V_K) + G_{Lk,x} \times (V_m - V_{LK}), \tag{11}$$

$$I_{mx} = G_{m,x} \times (V_m - V_x), \tag{12}$$

and

$$I_c = G_c \times (V_m - V_c). \tag{13}$$

The *m* and *x* indexes refer to soma and axon, respectively. For a more compact representation, the differential equations describing the dynamics of ion channels (equations 5, 6, 8, and 9) were written in vectorial form. The

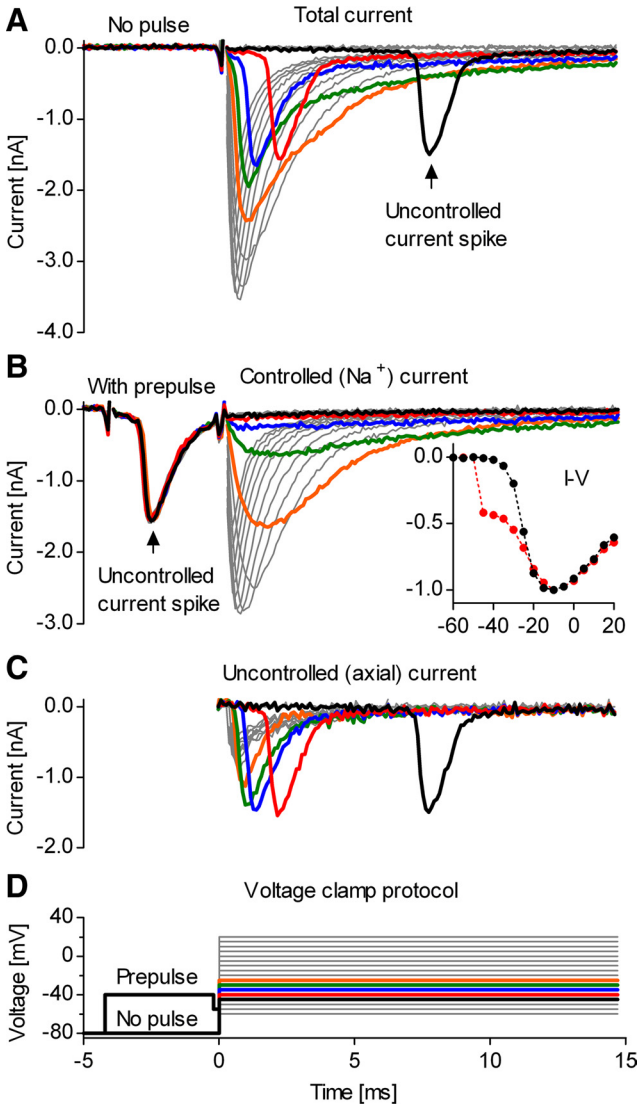

Figure 1. A voltage prepulse isolates the somatic Na^+ current from neurons in slices. Whole-cell voltage-clamp recording from a midline raphé neuron in a medullary slice. ***A***, Steps above −50 mV evoke out-of-control current spikes. Thick traces denote currents obtained at command potentials from −45 (black) to −25 mV (orange). ***B***, A brief pulse to −40 mV intentionally triggers the out-of-control spike and isolates the somatic Na^+ current. The inset shows the normalized peak current versus voltage, with (black plots) and without prepulse (red plots). The prepulse restores the typical aspect of the I-V curve. ***C***, Axial current, obtained by subtracting the currents in ***B*** from the currents in ***A***. ***D***, Voltage-clamp step protocol, with and without prepulse. To reduce the size of Na^+ currents, the internal solution contained 50 mM Na^+. Traces in ***A*** and ***B*** show TTX-sensitive current obtained by subtracting currents recorded before and after application of 1 μM TTX.

P values are the state probability vectors, and the **Q** values are the voltage-dependent rate matrices (Colquhoun and Hawkes, 1995). The G_{Na}, G_K, and G_{Lk} values are the conductances for Na_v and K_v channels and for the leak. The P_O values are the instantaneous open probabilities for Na_v and K_v channels. V_{Na}, V_K, and V_{Lk} are the reversal potentials for Na^+, K^+, and leak currents. G_{mx} is the electrical conductance between soma and axon ($G_{mx} = 1/R_{mx}$). The I_C value represents current injected into the soma. In voltage clamp, I_C is the current injected to clamp the voltage in the soma, where V_c is the command voltage and G_c is a voltage-clamp gain factor. In current clamp, $G_c = 0$. To make results easier to interpret, we made $R_s = 0$ in all simulations.

Simulations. Both current-clamp and voltage-clamp simulations were obtained by integrating numerically the differential equations 4–9. We used an integration method as described previously (Milescu et al., 2008). Briefly, equations 4 and 7 were integrated using Euler's method:

$$V_{m,t+dt} = V_{m,t} + dt \times (-I_m - I_{mx} - I_c)/C_m, \quad (14)$$

and

$$V_{x,t+dt} = V_{x,t} + dt \times (-I_x + I_{mx})/C_x, \quad (15)$$

where dt is the sampling time (10 μs). Simultaneously, equations 5, 6, 8, and 9 were integrated in matrix form, using the following solution:

$$\mathbf{P}_{t+dt} = \mathbf{P}_t \times e^{\mathbf{Q}(V_t)\times dt}, \quad (16)$$

where **P** stands for $\mathbf{P}_{Na,m}$, $\mathbf{P}_{Na,x}$, $\mathbf{P}_{K,m}$, or $\mathbf{P}_{K,x}$, **Q** stands for $\mathbf{Q}_{Na}$, or $\mathbf{Q}_K$, and V_t stands for $V_{m,t}$ or $V_{x,t}$. The quantities $e^{\mathbf{Q}\times dt}$ were precalculated over a voltage range from −100 to +100 mV (every 0.1 mV) using the spectral expansion method (Colquhoun and Hawkes, 1995). At each integration step, the appropriate **Q** matrices were chosen according to the values of $V_{m,t}$ and $V_{x,t}$. The parameters used in the simulations are given in supplemental Table 1, available at www.jneurosci.org as supplemental material.

Results

The somatic Na^+ current can be isolated with a voltage prepulse

An example of whole-cell Na^+ currents recorded from midline raphé neurons in medullary slices (Ptak et al., 2009) is presented in Figure 1*A* in response to a typical voltage-clamp step protocol (Fig. 1*D*). The experimental conditions were optimized for isolating Na^+ currents as described in Materials and Methods. As is typical for voltage clamp of intact neurons, the recorded current shows clear signs of poor voltage control, with voltage steps positive to −50 mV abruptly activating large spikes of inward current. These likely reflect the triggering of out-of-control action potentials in the axon. With increasing voltage in the range from −45 to −20 mV, the spike of inward current has similar magnitude but occurs earlier. The spike appears to be superimposed on a component of Na^+ current that increases more gradually with voltage, as is expected for a somatic Na^+ current under good voltage control. At potentials positive to −20 mV, the distinction between spike and somatic Na^+ current is less clear, since they appear to overlap. These records are similar to those in previous recordings of whole-cell Na^+ currents from central neurons *in situ* (Barrett and Crill, 1980; Magistretti et al., 2006; Goldfarb et al., 2007), where the same interpretation of an axonal spike riding on top of well controlled somatic currents was proposed.

We tested whether intentionally triggering the axonal spike could inactivate the axonal channels and leave only somatic channels available for activation. For this, a brief voltage prepulse to −40 mV, which activated the current spike, was introduced in the step protocol. As a result, it appears that the subsequent voltage steps evoke only Na^+ current under good space clamp (Fig. 1*B*). Thus, the prepulse eliminates the distorting effect that the uncontrolled current spike has upon the current versus voltage relation (Fig. 1*B*, inset). Assuming that the prepulse inactivates Na_v channels in the axon and eliminates the axial current flowing from axon to soma, the axial current can be isolated from the total measured current by subtracting the current obtained with prepulse (Fig. 1*B*) from the current obtained without prepulse (Fig. 1*A*). The result is presented in Figure 1*C*.

The voltage prepulse selectively inactivates axonal Na_v channels

To understand the effect of the voltage prepulse, we constructed a reduced computational neuron model consisting of only two iso-

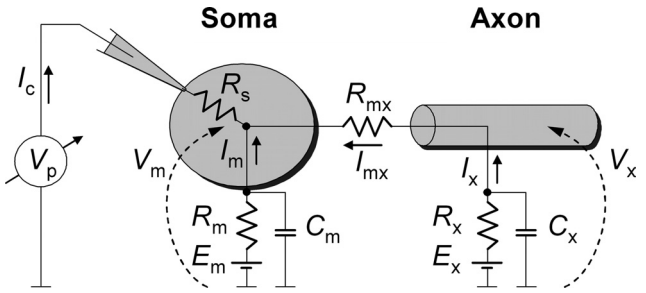

Figure 2. Reduced neuron compartmental model. A model consisting of only two compartments (soma and axon) individually isopotential and electrically connected through a resistor (R_{mx}). An axial current I_{mx} flows between axon and soma whenever they are not equipotential ($V_m \neq V_x$). In a typical voltage-clamp configuration, the clamping current I_c is injected in the soma to keep the somatic potential V_m equal to a command voltage. According to this model, the injected current I_c is equal to the sum of somatic current I_m and axial current I_{mx}. R_m and R_x represent the totality of somatic and axonal ionic conductance with overall reversal potentials E_m and E_x, respectively. C_m and C_x are the capacitances of the somatic and axonal membranes, respectively. The access resistance R_s makes the voltage measured at the pipette V_p differ from the somatic voltage V_m.

potential compartments: the soma and the axon (Fig. 2). Although this compartmental model is greatly simplified (cf. Yu et al., 2008), it served well the purpose of our study and its properties can be easily understood. The two compartments were populated with identical conductances: a Na_v channel, a K_v channel, and a leak conductance. The parameters of the compartmental model (supplemental Tables 1 and 2, available at www.jneurosci.org as supplemental material) were tuned to generate spontaneous spiking (supplemental Fig. 1, available at www.jneurosci.org as supplemental material) resembling the activity of raphé neurons (Jacobs and Azmitia, 1992; Ptak et al., 2009). The density of Na_v channels was made ~10 times greater in the axon than in the soma (Kole et al., 2008); we also tried a configuration in which axonal and somatic densities were equal but axonal Na_v channels had voltage sensitivity 10 mV more negative (Colbert and Johnston, 1996).

The compartmental model was simulated in response to a voltage-clamp step protocol (Fig. 3). The currents obtained with and without the prepulse qualitatively match the experimental data shown in Figure 1. To clamp the membrane potential during a voltage-clamp experiment, the amplifier injects current into the soma through a relatively small access resistance (Fig. 2, R_s). In contrast, the current enters the axon through a much larger resistance (Fig. 2, R_{mx}). Thus, only the soma is effectively voltage clamped, whereas the axon is not (Fig. 3*A*, somatic potential vs axonal potential). Without a voltage prepulse (Fig. 3*A*), command voltage steps above −50 mV trigger axonal spikes. The initiation and the depolarization phase of these spikes are caused by axonal Na_v channels. As K_v channels are "blocked" in the simulation, the downstroke is caused by the hyperpolarizing axial current flowing from the soma, which is more negative. The total current measured by the amplifier is the sum of somatic Na$^+$ current and axial current.

The voltage prepulse to −40 mV causes enough axonal depolarization and is long enough (4 ms) to trigger an axonal spike (Fig. 3*B*, axonal potential). During the spike, the axonal potential reaches positive values, causing axonal Na_v channels to inactivate quickly and almost completely (Fig. 3*B*, axonal channel availability). In contrast, somatic Na_v channels inactivate very little (Fig. 3*B*, somatic channel availability), because the somatic potential remains at −40 mV (Fig. 3*B*, somatic potential). Because of the very small axonal Na_v channel availability remaining after the prepulse, the axon behaves as a passive structure and the voltage steps following the pulse can no longer trigger spikes (Fig. 3*B*, axonal potential). Since now the axon and soma are approximately equipotential, the axial current is very small during the steps (Fig. 3*B*, axial current), and the current measured by the amplifier (excluding capacitive transients) is approximately equal to the somatic Na$^+$ current (Fig. 3*B*, total current vs somatic Na$^+$ cur-

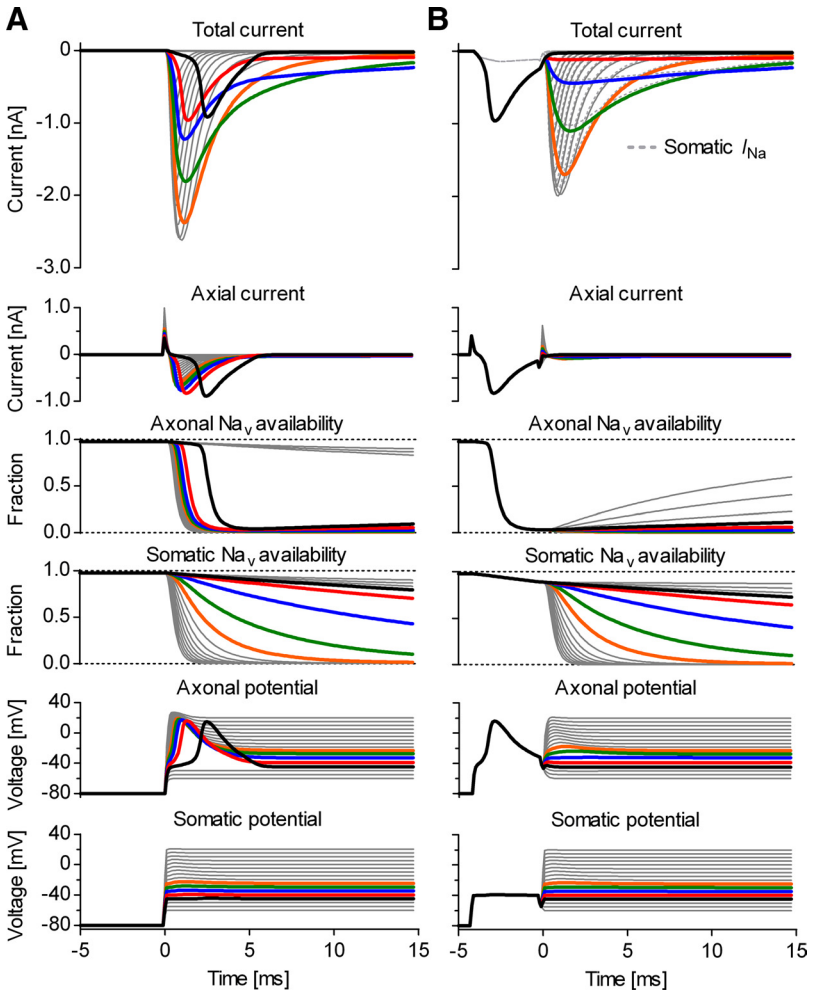

Figure 3. The voltage prepulse selectively inactivates axonal Na_v channels in model simulations. Voltage-clamp simulation of the compartmental model, shown in Figure 2, in response to a step protocol without (***A***) or with prepulse (***B***). ***A***, Without the prepulse, voltage steps above −50 mV trigger axonal spikes, causing axial current (Fig. 2, I_{mx}) to overlap with somatic Na$^+$ current. ***B***, The prepulse intentionally triggers the axonal spike, which selectively inactivates axonal Na_v channels but has little effect on somatic channels. During the subsequent voltage step, the soma and the axon are approximately equipotential and the total ("measured") current is approximately equal to the somatic Na$^+$ current (gray dotted lines). The capacitive transients were subtracted from the total current. The thick traces denote quantities at command potentials from −45 (black) to −25 mV (orange).

rent). We also simulated a situation with equal axonal and somatic densities but with more negative voltage dependence for the axonal channels and obtained qualitatively similar results (data not shown).

Optimal isolation of somatic Na^+ currents

To optimally isolate the somatic Na^+ current from the axial current, the prepulse can be optimized to suit individual neurons or different neuronal types by using test protocols such as those shown in Figure 4. In choosing the voltage and duration of the prepulse, one should consider several issues. Most importantly, the voltage should be sufficiently depolarizing to quickly trigger an axonal spike (Fig. 4*A*,*C*). In our experience, more positive potentials inactivate axonal Na_v channels more profoundly but also inactivate more somatic channels. Furthermore, the pulse should be long enough to allow completion of the axonal spike when the soma and axon become approximately equipotential and the axial current is null. However, especially in neurons with very large axonal channel density, longer pulses may result in increased axial current or may even trigger further axonal spikes by allowing axonal channels to partially recover from inactivation. Finally, the prepulse should be followed by a brief hyperpolarization to allow partially activated somatic channels to deactivate. This hyperpolarization should not be too long or too negative, as it may also result in axonal channel recovery (Fig. 4*B*,*D*).

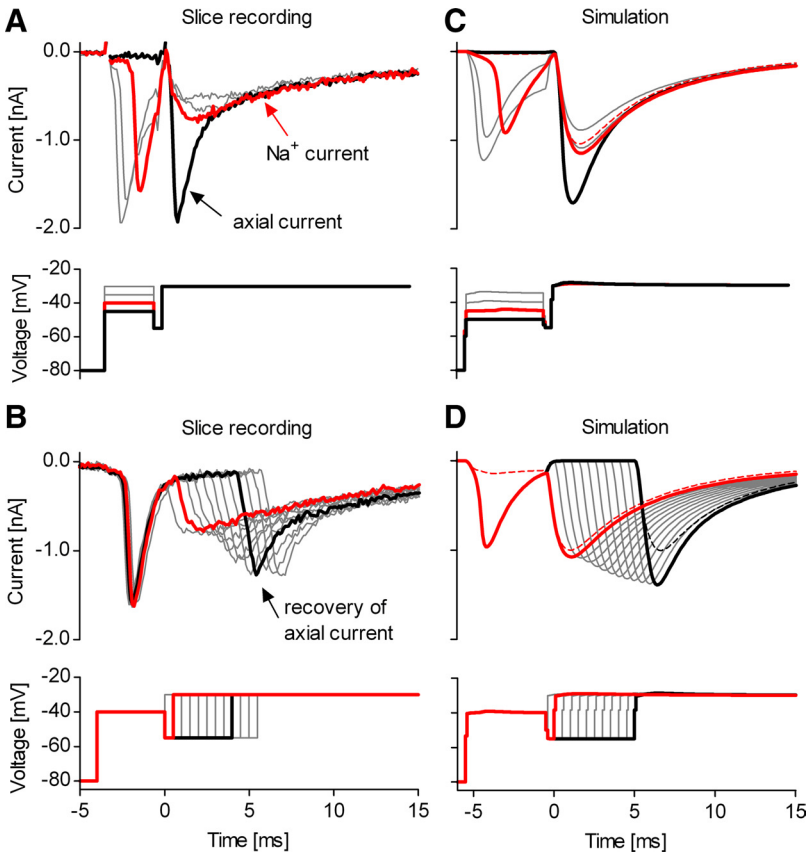

Figure 4. Optimal isolation of somatic Na^+ currents. Two voltage-clamp protocols designed to determine optimal conditions for axial current removal. Illustrative data obtained from the same neuron as shown in Figure 1. ***A***, The prepulse potential should be chosen as the minimum voltage that quickly evokes the uncontrolled current spike (−40 mV). A relatively low test potential (−30 mV) should result in a current with smooth rise and approximately single exponential decay (red trace). ***B***, The axial current, initially eliminated by the prepulse, recovers within a few ms at −55 mV. ***C*** and ***D***, Simulations of the compartmental model, shown in Figure 2, in response to voltage-clamp protocols similar to those in ***A*** and ***B***, respectively. The dashed red lines represent the somatic Na^+ current, approximately equal to the total ("measured") current. The internal solution contained 50 mM Na^+, and traces were TTX subtracted.

In the example shown in Figure 4*B*, the red trace corresponds to an optimal prepulse: 4 ms at −40 mV, followed by 0.5 ms at −55 mV. Under these conditions, the current evoked by the step to −30 mV appears to be well controlled, as indicated by the smooth decay. Generally, current decay with a single exponential time course at voltages where inactivation is slow compared with the decay of axial current (≈−30 mV) is a good indicator that the axial current has been eliminated. However, an additional fast inactivating component may genuinely occur, either as a result of intrinsic kinetic properties or as an effect of Na_v channel heterogeneity. In some cases, it might be useful to apply a train of prepulses instead of a single pulse to force axonal Na_v channels into inactivated states characterized by slow recovery (Mickus et al., 1999).

The prepulse is effective in other neuronal types

We tried the prepulse technique in a large number of brainstem raphé neurons ($n > 50$). Although difficult to quantify, the prepulse left no visible evidence of space-clamp errors in a large fraction (>50%) and generally improved space clamp in all neurons. An example of very good correction was shown in Figure 1. It is possible that, for whatever reasons, raphé neurons are particularly amenable to the prepulse technique. Therefore, we tested other neuronal types as shown in Figure 5, namely cortical pyramidal neurons (Fig. 5*A*), brainstem neurons in the inferior olivary nucleus (Fig. 5*B*), and motoneurons in the hypoglossal (XII) nucleus (Fig. 5*C*). With pyramidal neurons ($n = 13$), the prepulse was effective in 9/13 and partially effective in 3/13 cells (when partially effective, the prepulse leaves some axial current and visibly distorts the recorded currents). With olivary neurons ($n = 4$), the prepulse was effective in 3/4 and partially effective in 1/4 cells. With motoneurons ($n = 6$), the prepulse was effective in 4/6 and partially effective in 2/6 cells.

Na^+ currents isolated from neurons in slices resemble currents recorded from dissociated neurons

The examples presented in Figures 1 and 5 demonstrate that the axial current spike can be eliminated with a well timed voltage prepulse. However, a control experiment is necessary to determine whether the current recorded after the prepulse is still distorted by residual axial current or by other artifacts. For this test, the Na^+ currents isolated from neurons in slices can be compared against the Na^+ currents recorded from preparations that are normally under good space-clamp control, such as outside-out or nucleated patches or acutely dissociated neurons. Of these possibilities, we chose dissociated neurons, because they are physiologically the closest to intact neurons in slice preparations. Furthermore, we chose cortical pyramidal neurons, because they can be more easily identified (under IR-DIC) in slices and in

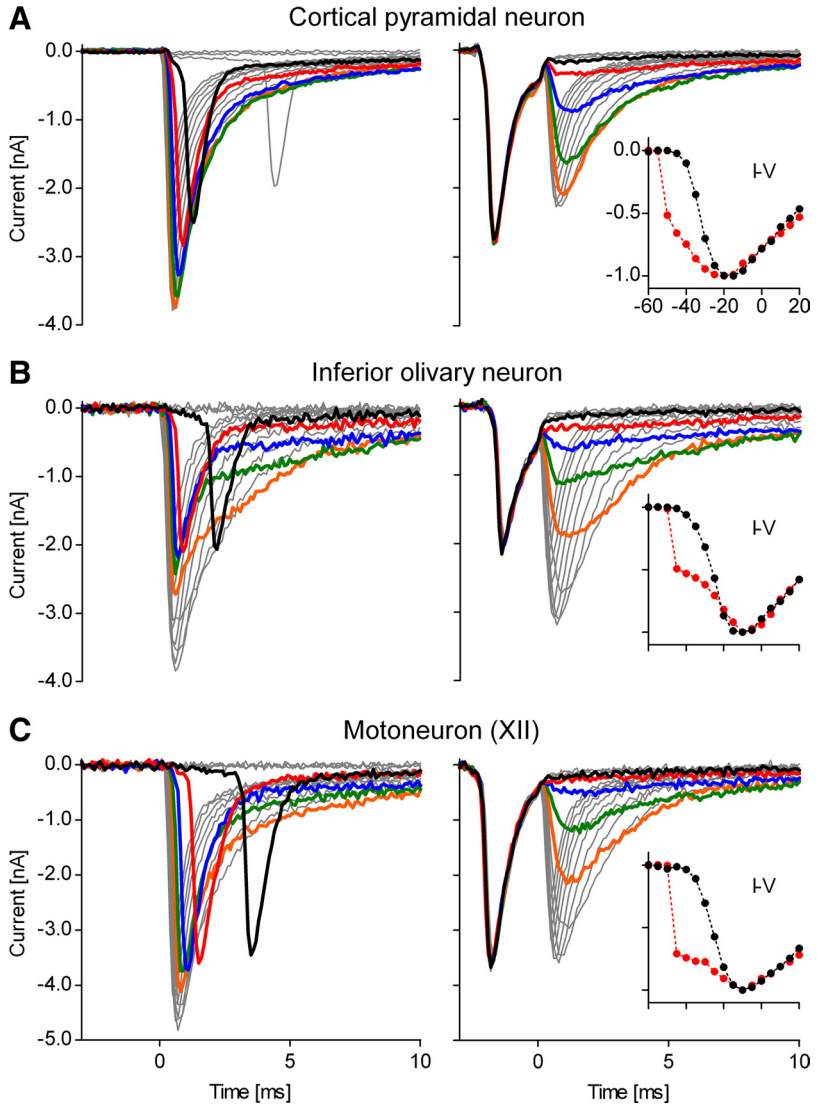

Figure 5. The voltage prepulse is effective in other neuronal types. ***A–C***, Illustrative examples showing somatic Na^+ current isolation in other neuronal types in slices of cortical pyramidal neurons (***A***), brainstem inferior olivary neurons (***B***), and brainstem hypoglossal (XII) motoneurons (***C***). The data were obtained without prepulse (left panels) or with prepulse (right panels). In all these examples, the prepulse eliminates the uncontrolled current spike. The thick traces denote quantities at command potentials from −45 (black) to −25 mV (orange). The insets are I-V curves with (black plots) and without prepulse (red traces). The currents in ***B*** and ***C*** were recorded with subsaturating TTX (50 nM) to reduce Na^+ current magnitude. In all cases, the internal solution contained 50 mM Na^+. All traces were TTX subtracted.

acute dissociations, thanks to their larger size and particular morphology. To make the comparison as precise as possible, the two sets of recordings (slice and dissociated) were obtained under identical experimental recording conditions (solutions, electrodes, temperature, etc.).

The average properties of Na^+ currents obtained from the two preparations are very similar, as illustrated by the examples shown in Figure 6. The current–voltage relation for peak Na^+ current measured in slices using the prepulse method is essentially identical to that measured in acutely dissociated neurons (Fig. 6*B*, inset). The only noticeable difference between the Na^+ currents recorded in the two preparations was in the kinetics of inactivation. In both cases, the time course of inactivation was biexponential, as is typical for Na^+ currents recorded from central neurons (e.g., Sah et al., 1988; Magee and Johnston, 1995), and with both preparations there was cell to cell variability in kinetics. However, there was a slightly larger contribution of a more slowly decaying component in currents isolated from slices using the prepulse than in those recorded from dissociated neurons (Fig. 6, *A* vs *B*). This could reflect slight differences in Na_v channel kinetics between dendrites and soma, or it could reflect contributions of current from parts of the dendrite not perfectly isopotential with the soma.

In principle, the voltage prepulse itself might alter the shape of the Na^+ current by changing the initial state occupancy of Na_v channels. However, we determined that this is not the case, as illustrated by the examples shown in Figure 7. Thus, Na^+ currents recorded from dissociated neurons without (Fig. 7*A*) and with (Fig. 7*B*) a voltage prepulse are virtually identical, apart from a proportional reduction in size (10–20%) caused by partial inactivation during the prepulse. From these results, it can also be inferred that currents isolated from neurons in slices using the prepulse are representative of the real magnitude of somatic Na^+ currents.

Improved space clamp allows quantitative measurement of gating properties

The "tail" currents that flow during deactivation of Na^+ channels are especially rapid, with strongly voltage-dependent kinetics (Hodgkin and Huxley, 1952), and thus constitute a good test for the quality of voltage clamp. We therefore examined the kinetics of tail currents recorded from raphé neurons in slices before and after using a prepulse to inactivate axonal channels. We found that the voltage prepulse not only eliminates the uncontrolled axial current spike from slice recordings but also improves the quality of space clamp as reflected in the tail current kinetics (Fig. 8).

A typical tail current experiment consists in applying a brief depolarizing pulse to activate (open) the channels with minimal inactivation, followed by steps to more negative potentials, during which channels deactivate (close) with voltage-dependent kinetics (Fig. 8*A*). The activation pulse is too brief to trigger an out-of-control axial current spike. However, close examination reveals a nonexponential, distorted decay of the tail currents (Fig. 8*C*, red traces). In contrast, introducing a prepulse in the protocol triggers the axial current spike (Fig. 8*B*) and also results in faster and more regular decay of tail currents (Fig. 8*C*, black traces). Two exponential components can now be identified, of which the major one is fast and voltage dependent (denoted by τ_d). This major component (generally >80%) exhibits the expected exponential voltage dependence of Na_v channel deactivation (Fig. 8*D*), similar to tail currents recorded in outside-out patches (Martina and Jonas, 1997). The small slow component in the tail currents might reflect sodium channels present in dendrites in which the local potential follows the command voltage more slowly. This exper-

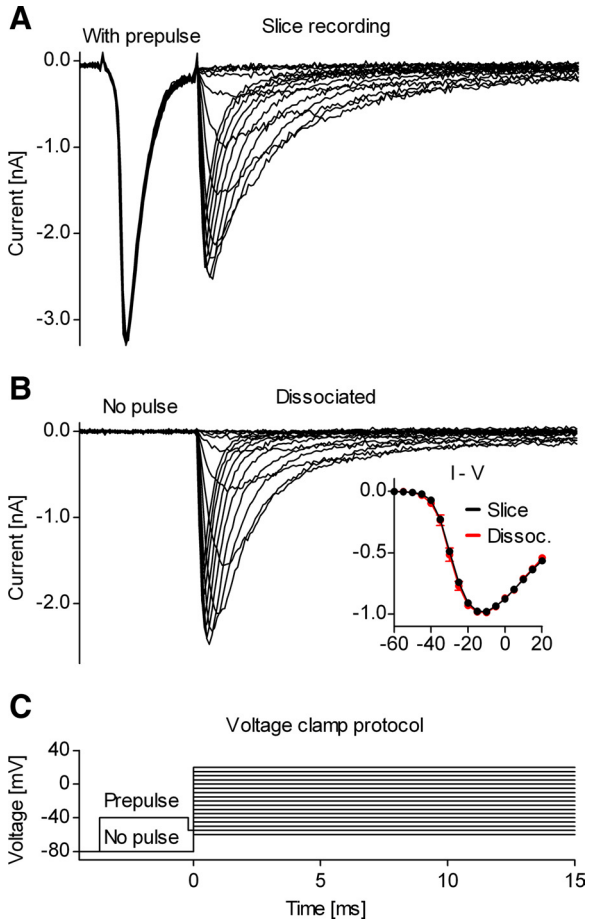

Figure 6. Na^+ currents isolated from neurons in slices resemble currents from dissociated neurons. ***A***, ***B***, Examples of Na^+ currents recorded in a cortical slice from a pyramidal neuron in layer V (***A***) and a dissociated cortical pyramidal neuron (identification based on morphology) (***B***). The inset in ***B*** contains I-V curves obtained from neurons in slices (mean values and SD, $n = 20$, black plots) and from dissociated neurons (Dissoc.) ($n = 8$, red plots). These traces were recorded with internal solutions containing 13 mM Na^+. The traces in ***A*** used TTX subtraction to isolate sodium current. In ***B***, sodium current was isolated by leak subtraction using the P/n protocol. ***C***, Voltage-clamp protocol.

iment also allows an estimate of how quickly the voltage clamp is established in the soma, since any delay would show up as a lag before the rapid decay of the current. This lag was ≈100 μs.

Discussion

The prepulse technique presented here is extremely simple but dramatically improves space-clamp conditions for recording Na^+ currents in neurons with intact morphology. Although the results will undoubtedly vary across individual neurons and neuronal types, we have demonstrated that the prepulse is effective in cells of different types (Figs. 1 and 5) and provides good quality data in a significant fraction of the cells tested at no cost. Previously, transient Na^+ currents with apparently good voltage control have been recorded from only a few cell types in brain slices. Magistretti et al. (2006) were able to obtain recordings with well controlled Na^+ currents from cerebellar granule neurons in brain slices, but only in ≈15% of the cells they tested. Enomoto et al. (2007) were able to record well controlled Na^+ currents from mesencephalic trigeminal neurons using very low (15 mM) external Na^+ to improve voltage control. However, in our recordings from a total of >70 neurons of other types, including cortical pyramidal neurons, inferior olivary cells, raphé neurons, and motoneurons in the hypoglossal (XII) nucleus, we never achieved good control unless the prepulse technique was used, even when current size was reduced with a partially blocking concentration of TTX (50 nM). In contrast, with the prepulse technique, good control could be achieved in 50–75% of the cells of each neuronal type tested. Thus, the technique seems likely to greatly increase the yield with which well controlled Na^+ currents can be obtained from a wide variety of neurons in brain slices.

Recording well controlled Na^+ currents directly from intact neurons in brain slice preparations has obvious advantages, but also some limitations. Most significantly, while inactivating axonal Na_v channels can eliminate obvious loss of voltage control, there is likely still imperfect uniformity of voltage between soma, axon, and dendrites. In this respect, acutely dissociated neurons or nucleated patches may provide cleaner data and better resolution of extremely fast kinetics (e.g., Kuo and Bean, 1994; Baranauskas and Martina, 2006).

Many central neurons, including cortical and hippocampal pyramidal neurons, contain Na^+ channels in the dendrites as well as soma and axon (Huguenard et al., 1989; Stuart and Sakmann, 1994; Magee and Johnston, 1995; Martina et al., 2000), and these channels can contribute significantly to the firing behavior of

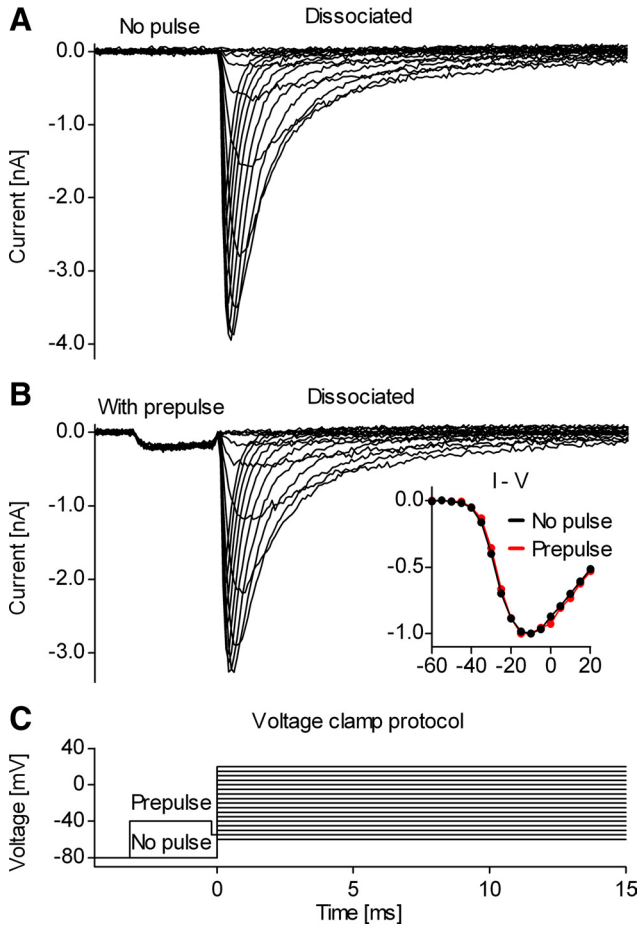

Figure 7. The voltage prepulse has minimal effects on somatic Na^+ currents. ***A***, ***B***, Example showing a comparison between Na^+ currents recorded from a dissociated cortical pyramidal neuron, without (***A***) or with (***B***) the voltage prepulse. There is limited activation and inactivation of Na_v channels during the prepulse causing only a small reduction in the current evoked by the subsequent voltage steps (***B***). The inset in ***B*** contains the I-V curve obtained without (black plots) or with (red plots) prepulse. The traces were recorded with internal solutions containing 13 mM Na^+ and were TTX subtracted. ***C***, Voltage-clamp protocol.

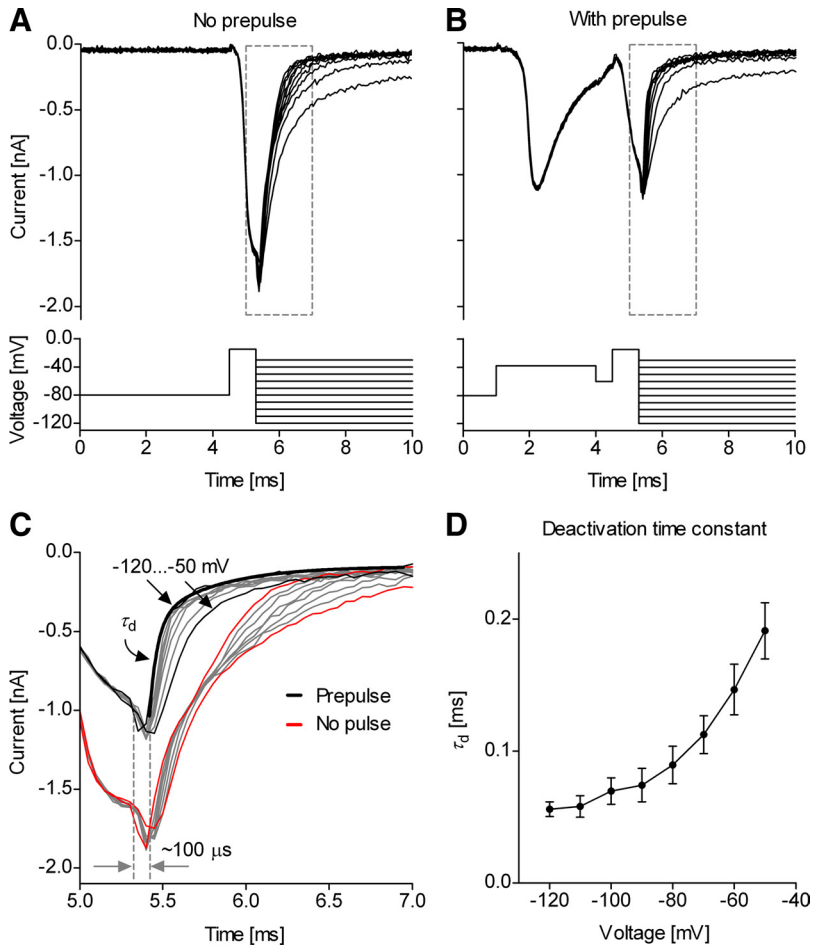

Figure 8. Improved space clamp allows quantitative measurement of deactivation. ***A***, ***B***, Example of Na^+ tail currents recorded in a medullary slice from a midline raphé neuron without (***A***) and with (***B***) a voltage prepulse. ***C***, Without prepulse, the decay of tail currents is distorted (red and gray traces); with prepulse, the tail currents decay exponentially (black and gray traces). The decay contains a fast component (τ_d) and a slower component. The thick black line is a two-exponential fit of the tail current at −120 mV. The tail currents respond with a relatively short lag (≈100 µs) to a step change in the command voltage. ***D***, The fast component τ_d is voltage-dependent (mean values and SD, $n = 7$). The traces were recorded using internal solution containing 50 mM Na^+ and were leak subtracted using the P/n protocol.

the neurons (e.g., Williams and Stuart, 1999; Yue et al., 2005). It is uncertain how much dendritic sodium channels contribute to the Na^+ current properties measured using our technique. There is a close similarity in the voltage dependence of activation between cortical neurons in brain slices (with prepulse) and dissociated neurons (Fig. 6), which suggests that most of the channels contributing to the measured current are electrotonically close to the soma (the point of current injection in voltage clamp). This is consistent with the idea that soma plus proximal dendrite can be well approximated by a single compartment model (Huguenard et al., 1989). The voltage of a more distal dendrite is likely to follow the command voltage more slowly than the voltage of the soma and proximal dendrite, but the distal dendrite will also contribute less current. Thus, a small contribution of membrane in distal dendrites could account for the small slower phase of tail current kinetics (Fig. 8). Also, the larger presence of a more slowly inactivating Na^+ current component in recordings made from cortical pyramidal neurons in slices (Fig. 6*A*), compared with dissociated neurons (Fig. 6*B*), could also result from imperfect isopotentiality. However, there may also be genuine differences in kinetics between channels in the soma, dendrites, and initial segment. There would be a larger contribution of dendritic currents in the *in situ* case than in dissociated cells and possibly a contribution in dissociated neurons from initial segment channels that have been "resorbed" into the dissociated cell body.

Extracting comprehensive kinetic information requires a variety of voltage-clamp protocols to be applied. However, the prepulse can be introduced only in some protocols, such as the step protocol shown in Figure 1, which informs about the time course and voltage dependence of activation and inactivation at suprathreshold potentials. Other examples include protocols for deactivation (Fig. 8, tail currents), resurgent current, or using the action potential as a voltage command. However, the prepulse may be only effective for tens of milliseconds, especially at more negative potentials, where axonal Na_v channels partially recover from inactivation and can regenerate uncontrolled axonal spikes. Thus, the prepulse is not useful for separating subthreshold or persistent Na^+ currents using very long voltage steps or slow ramps. In this case, one may consider blocking axonal channels with focal TTX application (e.g., Castelli et al., 2007).

Other examples where the prepulse cannot be used—at least not in a simple way—include protocols for voltage-dependent availability, development of inactivation, or recovery from inactivation. Combining these data, containing a mixture of Na^+ and axial current with prepulse-corrected currents could introduce some inconsistency that may result in modeling errors. Depending on the neuronal preparation, prepulse-free experiments may have to be experimentally optimized separately from the rest to minimize the contribution of the axial current to the total current. A conceivable alternative would be to somehow calibrate the axial current and subtract its predicted contribution from data recorded without the prepulse.

Depending on age and neuronal type, in our experiments Na^+ currents could reach amplitudes in excess of 10 nA. Even in preparations with ideal space clamp, such large currents are difficult to control as a result of series resistance errors. Thus, experiments using acutely dissociated neurons typically rely on reducing external Na^+ concentration (e.g., Raman and Bean, 1997; Royeck et al., 2008) or using subsaturating concentrations of TTX (e.g., Carter and Bean, 2009) to achieve good voltage control. We adopted a similar strategy in this study. In addition to achieving better voltage control, we found that reducing the Na^+ current with high internal Na^+ or subsaturating TTX also made the prepulse significantly more effective at improving space clamp. However, without the prepulse technique, poor space clamp always remained poor regardless of Na^+ current amplitude. The likely explanation is that, even when partially reduced, the remaining density of axonal Na^+ current may be so large that uncontrolled axonal spikes can still be generated (cf. Madeja, 2000). However, once an axonal spike is intentionally

triggered with the prepulse, it cannot be regenerated as quickly when the Na^+ current density has been reduced. In the case of neurons with high axonal Na_v channel density or with unfavorable electrotonic characteristics, reducing the Na^+ current may be a necessary condition for obtaining good space clamp, even with the prepulse. This was the case with all the recordings made from inferior olivary cells and hypoglossal neurons (Fig. 5*B*,*C*).

The prepulse technique may be very well suited to studying Na^+ currents in primary cell culture preparations as well as brain slices. For example, even though cultured cerebellar granule cell neurons have an electrotonically compact cell body, it is often difficult to control sodium currents because of regenerative spikes in neurites (Osorio et al., 2005; Goldfarb et al., 2007). The prepulse procedure may allow optimal voltage-clamp studies in this preparation, which allows easy transfection by RNA and DNA and is very well suited for studies of sodium channel molecular biology and cell biology (e.g., Goldfarb et al., 2007).

References

Baranauskas G, Martina M (2006) Sodium currents activate without a Hodgkin-and-Huxley-type delay in central mammalian neurons. J Neurosci 26:671–684.

Barrett JN, Crill WE (1980) Voltage clamp of cat motoneurone somata: properties of the fast inward current. J Physiol 304:231–249.

Bar-Yehuda D, Korngreen A (2008) Space-clamp problems when voltage clamping neurons expressing voltage-gated conductances. J Neurophysiol 99:1127–1136.

Carter BC, Bean BP (2009) Sodium entry during action potentials of mammalian neurons: incomplete inactivation and reduced metabolic efficiency in fast-spiking neurons. Neuron 64:898–909.

Castelli L, Biella G, Toselli M, Magistretti J (2007) Resurgent Na^+ current in pyramidal neurones of rat perirhinal cortex: axonal location of channels and contribution to depolarizing drive during repetitive firing. J Physiol 582:1179–1193.

Colbert CM, Johnston D (1996) Axonal action-potential initiation and Na^+ channel densities in the soma and axon initial segment of subicular pyramidal neurons. J Neurosci 16:6676–6686.

Colquhoun D, Hawkes AG (1995) A Q-matrix cookbook: how to write only one program to calculate the single-channel and macroscopic predictions for any kinetic mechanism. In: Single channel recording, 2nd Edition (Sakmann B, Neher E, eds), pp 589–636. New York: Plenum.

Diwakar S, Magistretti J, Goldfarb M, Naldi G, D'Angelo E (2009) Axonal Na^+ channels ensure fast spike activation and back-propagation in cerebellar granule cells. J Neurophysiol 101:519–532.

Edwards FA, Konnerth A, Sakmann B, Takahashi T (1989) A thin slice preparation for patch clamp recordings from neurones of the mammalian central nervous system. Pflügers Arch 414:600–612.

Enomoto A, Han JM, Hsiao CF, Chandler SH (2007) Sodium currents in mesencephalic trigeminal neurons from Nav1.6 null mice. J Neurophysiol 98:710–719.

Goldfarb M, Schoorlemmer J, Williams A, Diwakar S, Wang Q, Huang X, Giza J, Tchetchik D, Kelley K, Vega A, Matthews G, Rossi P, Ornitz DM, D'Angelo E (2007) Fibroblast growth factor homologous factors control neuronal excitability through modulation of voltage-gated sodium channels. Neuron 55:449–463.

Hamill OP, Marty A, Neher E, Sakmann B, Sigworth FJ (1981) Improved patch-clamp techniques for high-resolution current recording from cells and cell-free membrane patches. Pflügers Arch 391:85–100.

Hartline DK, Castelfranco AM (2003) Simulations of voltage clamping poorly space-clamped voltage-dependent conductances in a uniform cylindrical neurite. J Comput Neurosci 14:253–269.

Hodgkin AL, Huxley AF (1952) A quantitative description of membrane current and its application to conduction and excitation in nerve. J Physiol (Lond) 117:500–544.

Huguenard JR, Hamill OP, Prince DA (1989) Sodium channels in dendrites of rat cortical pyramidal neurons. Proc Natl Acad Sci U S A 86:2473–2477.

Jacobs BL, Azmitia EC (1992) Structure and function of the brain serotonin system. Physiol Rev 72:165–229.

Kole MH, Ilschner SU, Kampa BM, Williams SR, Ruben PC, Stuart GJ (2008) Action potential generation requires a high sodium channel density in the axon initial segment. Nat Neurosci 11:178–186.

Koshiya N, Smith JC (1999) Neuronal pacemaker for breathing visualized in vitro. Nature 400:360–363.

Kuo CC, Bean BP (1994) Na+ channels must deactivate to recover from inactivation. Neuron 12:819–829.

Madeja M (2000) Do neurons have a reserve of sodium channels for the generation of action potentials? A study on acutely isolated CA1 neurons from the guinea-pig hippocampus. Eur J Neurosci 12:1–7.

Magee J, Johnston D (1995) Characterization of single voltage-gated Na^+ and Ca2+ channels in apical dendrites of rat CA1 pyramidal neurons. J Physiol 487:67–90.

Magistretti J, Castelli L, Forti L, D'Angelo E (2006) Kinetic and functional analysis of transient, persistent and resurgent sodium currents in rat cerebellar granule cells in situ: an electrophysiological and modelling study. J Physiol 573:83–106.

Martina M, Jonas P (1997) Functional differences in Na^+ channel gating between fast-spiking interneurones and principal neurones of rat hippocampus. J Physiol 505:593–603.

Martina M, Vida I, Jonas P (2000) Distal initiation and active propagation of action potentials in interneuron dendrites. Science 287:295–300.

Mickus T, Jung H, Spruston N (1999) Properties of slow, cumulative sodium channel inactivation in rat hippocampal CA1 pyramidal neurons. Biophys J 76:846–860.

Milescu LS, Ptak K, Mogri M, Yamanishi T, Smith JC (2008) Real-time kinetic modeling of voltage-gated ion channels using dynamic clamp. Biophys J 95:66–87.

Osorio N, Alcaraz G, Padilla F, Couraud F, Delmas P, Crest M (2005) Differential targeting and functional specialization of sodium channels in cultured cerebellar granule cells. J Physiol 569:801–816.

Ptak K, Yamanishi T, Aungst J, Milescu LS, Zhang R, Richerson GB, Smith JC (2009) Raphé neurons stimulate respiratory circuit activity by multiple mechanisms via endogenously released serotonin and substance P. J Neurosci 29:3720–3737.

Rall W, Segev I (1985) Space-clamp problems when voltage clamping branched neurons with intracellular microelectrodes. In: Voltage and patch-clamping with microelectrodes (Smith TG Jr, Lecar H, Redman SJ, eds), pp 191–215. Bethesda, MD: American Physiological Society.

Raman IM, Bean BP (1997) Resurgent sodium current and action potential formation in dissociated cerebellar Purkinje neurons. J Neurosci 17: 4517–4526.

Royeck M, Horstmann MT, Remy S, Reitze M, Yaari Y, Beck H (2008) Role of axonal NaV1.6 sodium channels in action potential initiation of CA1 pyramidal neurons. J Neurophysiol 100:2361–2380.

Sah P, Gibb AJ, Gage PW (1988) The sodium current underlying action potentials in guinea pig hippocampal CA1 neurons. J Gen Physiol 91:373–398.

Spruston N, Jaffe DB, Williams SH, Johnston D (1993) Voltage- and space-clamp errors associated with the measurement of electrotonically remote synaptic events. J Neurophysiol 70:781–802.

Stuart GJ, Sakmann B (1994) Active propagation of somatic action potentials into neocortical pyramidal cell dendrites. Nature 367:69–72.

Stuart G, Schiller J, Sakmann B (1997) Action potential initiation and propagation in rat neocortical pyramidal neurons. J Physiol 505:617–632.

White JA, Sekar NS, Kay AR (1995) Errors in persistent inward currents generated by space-clamp errors: a modeling study. J Neurophysiol 73:2369–2377.

Williams SR, Stuart GJ (1999) Mechanisms and consequences of action potential burst firing in rat neocortical pyramidal neurons. J Physiol 521:467–482.

Yu Y, Shu Y, McCormick DA (2008) Cortical action potential backpropagation explains spike threshold variability and rapid-onset kinetics. J Neurosci 28:7260–7272.

Yue C, Remy S, Su H, Beck H, Yaari Y (2005) Proximal persistent Na^+ channels drive spike afterdepolarizations and associated bursting in adult CA1 pyramidal cells. J Neurosci 25:9704–9720.